International Journal of Innovative Technology and Exploring Engineering (IJITEE)
ISSN: 2278-3075 (Online), Volume-8 Issue-4, February 2019

Detection and Analysis of Cycle Slips from GNSS Observations

T. Raghavendra Vishnu, D. Venkata Ratnam, P. Bhanu Priyanka, M. Sridhar, K. Padma Raju

Abstract: ***Global Positioning System (GPS) receiver's high precision and high reliability has gained importance in recent years as a result of continuous demand for GPS applications in various fields. In order to obtain accurate positioning information the GPS receivers use carrier phase measurements for high-precision applications. Carrier phase measurements are greatly affected by Cycle Slips (CS). In this paper, detection of the cycle slips analysis is carried out using the raw carrier phase data recorded for the solar maximum year 2013 at Koneru Lakshmaiah (K L) University, Guntur, India. Higher-order phase differencing scheme is used for the detection of the cycle slips. At higher-order differences, the amplification of sudden jumps associated with the cycle slips can be observed thereby improving the ability to detect cycle slips. It is found that cycle slips occurrence is high during the solar maximum year (2013). The connection of cycle slip occurrence with ionospheric scintillations is also investigated. During the geomagnetic storm event on 29 June, 2013, maximum S4 has been observed due to fall in C/N0 leading to occurrence of cycle slips. Empirical Mode Decomposition-Detrended Fluctuation Analysis (EMD-DFA) algorithm is used for mitigating the effects of ionospheric scintillations.***

Index Terms: Cycle slips, EMD-DFA, Scintillations

I. INTRODUCTION

. Global Navigational Satellite System (GNSS) is being used for intense monitoring of the ionosphere and space weather. Random electron density structures in the ionosphere gives rise to rapid fluctuations of amplitude and phase in the received GNSS signal which leads to loss of lock and a delay in reacquiring the signal. Cycle slips in phase measurements limits the positional accuracy of GNSS users. Carrier phase measurements are more precise than code measurements [*Hoffmann-Wellenhof et al*., 1994]. The C/A code data of 1.023 Mbps signal provides an accuracy of around 1msec only whereas with carrier phase measurements an accuracy of around nanoseconds can be achieved. Code phase measurements are more affected by multipath when compared to carrier phase measurements. Apart from initial integer ambiguity, the major challenge faced by carrier phase measurements is cycle slip. Loss of lock in the GPS receiver causes a loss of count in the integer number of cycles in the carrier phase measurements and this results in a sudden jump in carrier phase measurements, and are known as cycle slips [*Leick et al*., 2015]. The three main factors responsible for the loss of lock of the GPS signal are, firstly, due to obstruction caused by trees and buildings, secondly, low Signal Noise Ratio (SNR) due to amplitude scintillation and low elevation angle. Lastly, failure in the receiver software and antenna also causes the incorrect signal processing [*Skone et al*., 2001]. Standalone GNSS receiver can track 10 to 12 satellites in the open sky condition whereas due to multipath and low elevation angle the SNR degrades substantially and tracking efficiency fall to about 7 to 9 satellites. During the strong multipath phenomena the number of visible satellites drops to 4 or 5. Standalone GNSS receiver is unsuitable for aircraft navigation due to problems in acquiring the carrier phase information as a result of the cycle slips [*Silva*, 2013]. *Blewitt et al*. [1990] developed an automatic editing algorithm where geometry-free combination and the melbourne-wubbena linear combination based on the threshold values were used to detect and correct the cycle slips. The algorithm was used in the software package GIPSY developed by the Jet Propulsion Laboratory (JPL), USA and BERNESE software developed by Institute of the University of BERN (AIUB) for detection and estimation of the cycle slips [*de Lacy et al*., 2008]. As India falls under low latitude region, ionospheric behavior is characterized by intense irregularities leading to scintillations and cycle slips. This alternates the need for augmentation systems such as Satellite-Based Augmentation System (SBAS) over the region of India prominently known as GAGAN (GPS Aided Geo Augmented Navigation). It mainly provides the services for the aircraft navigation system by providing accurate information during the aircraft landing. 25 GAGAN receivers are installed over a wide area network in the Indian Sub continent [*Sunda et al*., 2015]. Cycle slips occurrence degrades the performance of GNSS receivers. Therefore, several methods were implemented to detect the cycle slips [*Liu*, 2011; *Dai et al*., 2009; *Kim and Langley*, 2002; *Banville et al*., 2010]. The detection of cycle slip occurrence and its variation in relation to scintillation activity are analyzed over low latitude regions of China [*Zhang et al*., 2010]. Triple frequency method has been proposed for the detection of the cycle slips in BeiDou Navigation Satellite system (BDS) [*Zhao et al*., 2014]. COSMIC RO observations were analyzed the relationship of ionospheric weather and the occurrence of cycle slips [*Yue et al*., 2016]. Detection and correction of the cycle slips is still a challenging task, especially in the low latitude regions. In this paper, higher-order phase difference technique is applied for the detection of the cycle slips for the data recorded at low latitude regions of India using GNSS receiver and Empirical Mode Decomposition-Detrended Fluctuation Analysis (EMD-DFA) is implemented for mitigating the ionospheric scintillation effects.

Manuscript published on 28 February 2019.
***Correspondence Author(s)
T. Raghavendra Vishnu, Research Scholar, Department of ECE, KLEF, Guntur, India.
D.Venkata Ratnam, Professor, , Department of ECE, KLEF, Guntur, India.
P. Bhanu Priyanka, Asst Professor, Department of ECE, Andhra Loyola Institute of Engineering and Technology Vijayawada India
M. Sridhar, Professor, Department of ECE, KLEF, Guntur, India.
K. Padma Raju, Professor, Department of ECE ,JNTUK Kakinada, India

II. DATA PROCESSING

The data used for detection of the cycle slips has been collected from Novatel GPStation-6 GNSS receiver available at K L University (16.4415°N; 80.62179°E), Guntur. GNSS data of only 272 days were recorded at KLU for the year 2013 by the GPStation-6 receiver. The data on the rest of the days were not available due to system/power failure. In April, May, September and October months, only 18,13,18,15 days of data were recorded. In this paper cycle slips are detected using the phase higher order difference method. The order of difference depends on the motion of the receiver, the environment surrounding of the receiver where the measurements are made and the time interval between the adjacent epochs. The data collected using the GISTM receiver for the solar maximum year 2013 sampled at 30 secs in the RINEX format was considered for the detecting of the cycle slips.

III. CYCLE SLIP DETECTION ALGORITHM

Higher-order phase differencing method was used for detecting the cycle slips in carrier phase measurements. P-order difference operator Δ_t^p is applied to the previous n-epochs at the epoch time 't'. The carrier phase data sequence r(t) can be written as,

$$r(t)=\left[\Delta_{t-n+1}^{p}\,\emptyset_{Li}\,,\Delta_{t-n+2}^{p}\,\emptyset_{Li},\Delta_{t-n+3}^{p}\,\emptyset_{Li},\ldots..\Delta_{t}^{p}\,\emptyset_{Li}\right] \quad (1)$$

where $\emptyset_{Li}$ is the received carrier phase data measured in units of cycle.

Subscript L_i indicates the corresponding signal i.e., L1 (1575 MHz) or L2 (1227 MHz).

t is the observable interval or epoch.

Similarly applying the operator Δ_{t-1}^{p} at epoch time $t-1$ yields the data sequence $r(t-1)$ given as below

$$r(t-1)=\left[\Delta_{t-n+1}^{p}\,\emptyset_{Li},\Delta_{t-n+2}^{p}\,\emptyset_{Li},\ldots..\Delta_{t-1}^{p}\emptyset_{L_i}\right] \quad (2)$$

Algorithm

Step1: GPS RINEX data of navigation and observation date is considered as input to the cycle slip algorithm.

Step2: Calculate the mean of the data sequence $r\,(t-1)$, it is represented as M

$$M=\frac{\Delta_{t-n}^{p}\,\emptyset_{L_1}\;+\Delta_{t-n+1}^{p}\,\emptyset_{L_1}+\ldots\ldots+\Delta_{t-1}^{p}\emptyset_{L_1}}{n-1} \quad (3)$$

Step3: Calculate the standard deviation std1 for data sequence $r\,(t-1)$. The data sequence $r\,(t-1)$ is obtained without considering the current phase data at epoch 't' using the equation (2), it includes the phase data only up to the epoch '$t-1$'.

$$std1=\frac{\sqrt{\left(\Delta_{t-n+1}^{p}\,\emptyset_{L_1}-M\right)^2+\left(\Delta_{t-n+2}^{p}\,\emptyset_{L_1}-M\right)^2+\cdots\left(\Delta_{t-1}^{p}\,\emptyset_{L_1}-M\right)^2}}{\sqrt{n-1}} \quad (4)$$

Step4: Calculate the standard deviation $std2$ for the data sequence $r\,(t)$, it includes the new phase data or current phase data at epoch 't' also.

$$std2=\frac{\sqrt{\left(\Delta_{t-n+1}^{p}\,\emptyset_{L_1}-m\right)^2+\left(\Delta_{t-n+2}^{p}\,\emptyset_{L_1}\,m\right)^2+\ldots+\left(\Delta_{t}^{p}\,\emptyset_{L_1}-m\right)^2}}{\sqrt{n}} \quad (5)$$

where m is the mean of the data sequence $r(t)$.

Step5: Now calculate the deviation of the single element of the sequence, the current phase difference $\Delta_t^p\;\emptyset_{Li}$ from the mean 'M' of the data sequence $r(t-1)$. Deviation is denoted by D [*Dai*, 2012].

$$D=\Delta_t^p\;\emptyset_{L1}-M \quad (6)$$

The conditions that must be satisfied for the occurrence of the cycle slip are as follows

1. The standard deviation of r (t) must be compatible with the standard deviation of $r(t-1)$

$$\frac{std2}{std1} > Threshold$$

where threshold is set to 3 in the algorithm [*Dai*, 2012].

2. The current phase data component at epoch 't' should be matched with the mean of the $r(t-1)$.

$$D > 3\times std1$$

3. $D > 1$

If the above conditions are satisfied then the cycle slip is detected at the current epoch 't' otherwise it is a cycle slip free epoch.

IV. EMD-DFA ALGORITHM

Cycle slips are detected and quantified for K L University GNSS station data (year 2013). The scintillation affected satellites due to cycle slips are identified for carrying out ionospheric scintillation mitigation process on C/N_0 measurements. Empirical Mode Decomposition (EMD) algorithm is combined with Detrended Fluctuation Analysis (DFA), and this EMD-DFA technique is implemented for mitigating ionospheric scintillation effects on GNSS signals. EMD is used to analyze the non-stationary signals. EMD decomposes the signal into Intrinsic Mode Functions (IMFs) based upon the characteristics of the signal itself. EMD has wide applications in radar technology, fault diagnosis in roller bearings, biomedical engineering [*Dejie Yu et al*., 2003; *Yih Jeng et al*., 2007].

DFA algorithm can be used for analyzing the scaling properties and detection of the long-range correlations in the non-stationary data [*Kantelhardt et al*., 2002]. Using DFA technique the scaling exponent (α) is calculated, which is useful in eliminating the noise in the GPS signal. To obtain the scaling exponent (α) DFA technique is applied for each IMF obtained by EMD method as follows,

Step 1: Subtract the mean of the IMF from each sample of the data and integrate the obtained series.

Published By:
Blue Eyes Intelligence Engineering
and Sciences Publication (BEIESP)

$$y(i)=\sum_{i=1}^{t}\left[IMF(i)-\frac{1}{N}\sum_{k=1}^{N}IMF(k)\right] \quad (7)$$

where *N* is the length of each IMF.

Step 2: $y(i)$ is divided into N_p disjoint segments of same segment size p. For each segment a local trend is obtained by polynomial fitting technique. By subtracting polyfit function from corresponding segment we obtain the residue indicated as $m_u(i)$ for that particular segment, where $u=1,2,....,N_p;1\le i\le p$

Step 3: By calculating the root mean square value of the residue $m_u(i)$ we obtain the local detrended fluctuation function $F(u,p)$ for each segment. Finally, the overall fluctuation function $F(p)$ is obtained by taking the average of all the segments.

$$F(p)=\sqrt{\frac{1}{N_p}\sum_{u=1}^{N_p}[F(u,p)]^2} \quad (8)$$

Step 4: The detrended fluctuation function $F(p)$ and the timescale p are related by power-law as

$$F(p)\sim p^{\alpha} \quad (9)$$

where the Scaling exponent (α) is used for mitigating the scintillation noise based on the threshold.

V. RESULTS AND DISCUSSIONS

The GNSS receiver located at K L University, Guntur, India sited in the equatorial ionization anomaly zone at the low latitudes region provides RINEX navigation and observation data file for the analysis. 5.1 Cycle slip occurrence dependence on ionospheric scintillation

GPS signals are strongly affected by ionospheric scintillations. Strong scintillations lead to loss of lock in the receiver thereby causing difficulty in phase measurements due to sudden jump in an integer number of cycles. S4 index is a parameter commonly used to indicate the disturbances in the ionosphere. Figure 1 (a) shows the cycle slip occurrence count for PRN 15 satellite on June 29, 2013. On this day for PRN 15 satellite cycle slips occurrence was observed mainly during 17:00 and 18:00 Hrs Universal Time (UT) and this indicates a clear correlation between cycle slip occurrence and ionospheric scintillations. During the same time Carrier to Noise Ratio (C/N_0) for PRN 15 satellite decreases to 41dB due to degradation of the GPS signal as shown in Figure 1(b). Figure 1(c) shows the S4 index variation on June 29, 2013 for PRN 15 satellite and S4 index reaches a maximum of 0.8 at 18:00 Hrs (UT). Figure 1(d) shows the variation of Dst index on June 29, 2013. Dst index has fallen to -98 nT at 1:00 and 6:00 Hrs (UT) on June 29 due to occurrence of geomagnetic storm. For PRN 15 satellite data received on June 29, 2013 S4 index reached a maximum peak of 0.8 around 18:00 Hrs (UT) indicating very strong scintillation activity. Due to this, there is a fall in the C/N_0 ratio of the GPS signal, causing difficulty in tracking the signal by the receiver and hence resulting in the cycle slips occurrence during 18:00 Hrs(UT) as shown in Figure 1(a).

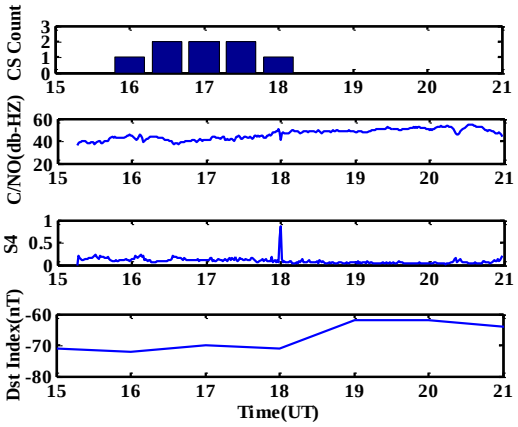

Figure 1. GNSS observations & geomagnetic indices on June 29, 2013 for PRN 15 satellite. (a) Cycle slip occurrence count (b) C/N_0 ratio (c) S4 Index (d) Dst.

5.2 Dependence of cycle slip occurrence on geomagnetic activity

Solar disturbances such as solar flares, coronal mass ejection affects the earth's magnetic field leading to geomagnetic storm. Disturbance Storm Time (Dst) index gives the measure of ring current of earth's magnetic field whereas, Ap index indicates the strength of geomagnetic activity for each 3 hour interval [*Saba et al.*, 1997]. Geomagnetic storm has occurred on June 29, 2013 during early hours causing significant changes in earth's magnetic field and disturbances in the ionosphere. Dst index value between -50 nT to -100 nT indicates moderate storm and greater than -100 nT indicates major storm. Figure 2(a) shows the variation of Dst index on June 29, 2013. Dst index has fallen to -98 nT at 1:00 and 6:00 Hrs (UT) on June 29 due to the occurrence of geomagnetic storm. Figure 2(b) gives the cycle slip occurrence count on the storm day June 29, 2013 where the cycle slip count is obtained by accumulating the CS occurrence for every 30-minute interval

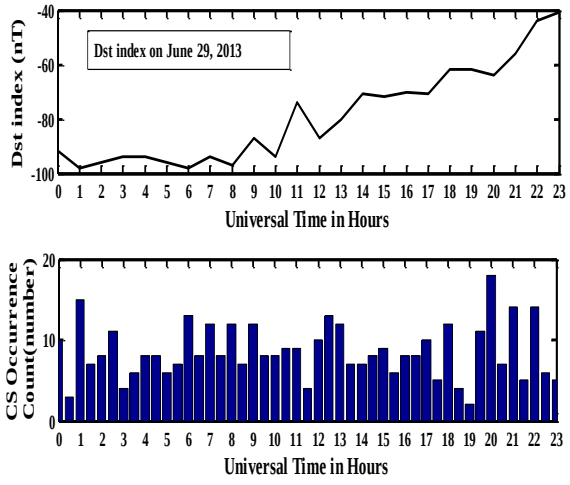

Figure 2. Geomagnetic index and cycle slips on storm date

Published By:
Blue Eyes Intelligence Engineering
and Sciences Publication (BEIESP)

June 29, 2013 (a) Dst index in nT on June 29, 2013 (b) Cycle slip occurrence count calculated at the interval of 30 minutes on June 29, 2013.

Figure 3(a) & (b) gives Dst index and Ap index variation for the solar maximum year 2013 respectively. Geomagnetic storms have occurred during the year on June 6, 28 and 29 and on March 27. Dst index has fallen to -79 nT,-66 nT around 180 and 152 dates of the year 2013 indicating geomagnetic disturbed conditions. Ap index has attained a peak value of 72 nT, 58 nT, 58 nT and 50 nT around 80,150, 275 and 180 dates of the year 2013 indicating a great change in geomagnetic activities on these days. It can be seen from the Figure 3(c) that more cycle slips are occurred during geomagnetic disturbed days (DOY 150,180 and 270). Cycle slip occurrence indicates the strength of the ionospheric irregularities. Increase in the level of geomagnetic activities leads to increase in the intensity of the TEC and therefore leading to signal degradation [*Afraimovich et al*., 2001].

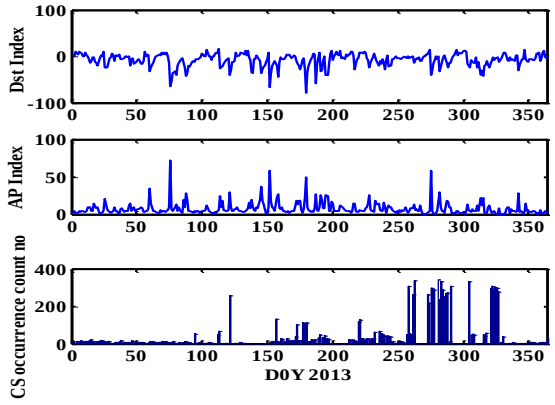

Figure 3. Geomagnetic indices and cycle slips count for the solar maximum year 2013. (a)Dst Index (b) Ap Index (c) Cycle slip occurrence count for each day of the year 2013.

5.3 Seasonal dependence of cycle slip occurrence

Figure 4 gives the number of detected cycle slips during each month of the solar maximum year 2013. Due to limited date availability during April and May, 2013 few cycle slips are detected.

The cycle slips are detected in the months of January (335), February (186) and December (116) months respectively, which are less when compared with the equinox months.

Table 1. Details of the number of cycle slip occurrences in the year 2013

Time in UT/Month	1 7:00 – 18:00	1 8:00 – 19:00	1 9:00 – 20:00	2 0:00 – 21:00	2 1:00 – 22:00	2 2:00 – 23:00	2 3:00 – 24:00	Total
January	85	47	16	33	71	71	12	335
February	15	22	51	56	23	18	1	186
March	71	66	30	26	7	8	6	214
April	50	23	34	29	45	38	19	238
May	40	51	51	54	52	43	7	298
June	137	153	113	169	193	185	62	1012
July	78	85	37	56	55	44	0	355
August	139	144	226	159	163	181	0	1012
September	197	280	311	196	262	182	2	1430
October	447	617	567	537	533	449	0	3150
November	364	435	403	359	343	412	129	2445
December	4	28	54	15	6	8	1	116
Total	\1627	1951	1893	1689	1753	1639	239	10791

The details of the cycle slips occurrences are summarized in Table 1 shown below. It is evident from the table that more cycle slips are detected during the autumn equinox period during the months of September, October and November when compared with the spring equinox months. Moreover, these cycle slips are observed more during evening period throughout the year. During the month of October, more cycle slips are detected when compared to other months followed by November and September respectively. During the solstice month June, more cycle slips are observed due to the occurrence of major geomagnetic storms during this month as shown in Figure 4. Equinox months September, October, March and April experience major scintillations when compared to solstice months [*Koster*, 1972].

January month is generally off season for the occurrence of scintillations or plasma bubble formations [*Burke et al*., 2004]. As during the equinox months scintillations occurrence is more when compared to solstice months, the occurrence of the cycle slips during equinox months is greater than solstice months. Figure 4 shows that the highest numbers of cycle slips are detected during the equinox months October and November of the solar maximum year 2013.

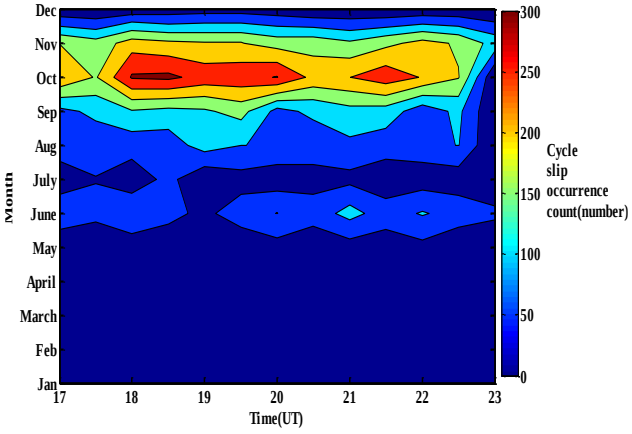

Figure 4. Cycle slip occurrence for every month of the solar maximum year 2013 during night time.

Cycle slips which are the results of signal blockage lead to considerable fall in the C/N_0 ratio. This fall in C/N_0 ratio is mitigated by applying EMD-DFA technique to the C/N_0 data received from the PRN 15 satellite on June 29, 2013. Figure 5 shows that 7 IMFs are obtained by applying EMD technique to C/N_0 data.

Published By:
Blue Eyes Intelligence Engineering and Sciences Publication (BEIESP)

IMF7 represents the residue. The local variations of the signal are extracted in the initial IMFs and the subsequent IMFs represent the significant signal content.

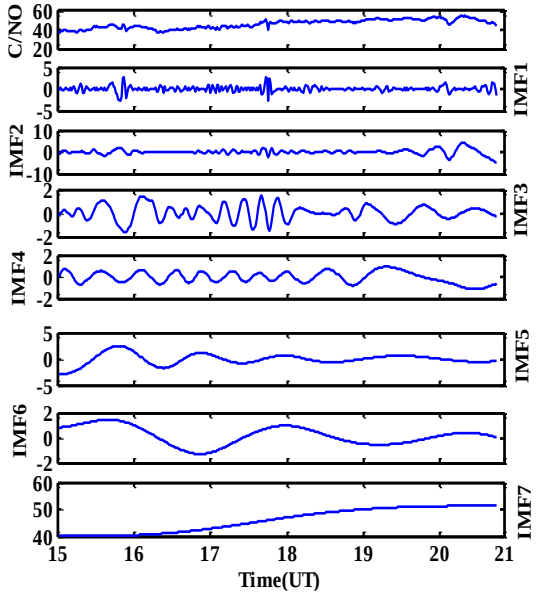

Figure 5. IMFs obtained by applying EMD technique to the C/N$_0$ time series received from PRN 15 satellite on June 29, 2013.

EMD gives better representation of the received C/N$_0$ time series data. DFA technique is applied for each of the IMF obtained by EMD method to the C/N$_0$ data. Figure 6 indicates the scaling exponent (α) values for the 7 IMFs by applying DFA technique. After applying DFA algorithm to the obtained IMFs, the IMFs 1, 2, 3 are not considered for the reconstruction of the original GPS signal as their Scaling exponent (α) values are below 0.5 which indicates scintillation noise. So, only IMFs 4,5,6,7 are considered for reconstruction of the original signal as their Scaling exponent (α) values are greater than 0.5 indicating that it is persistent or noise free data [*Tanna and Pathak*, 2014].

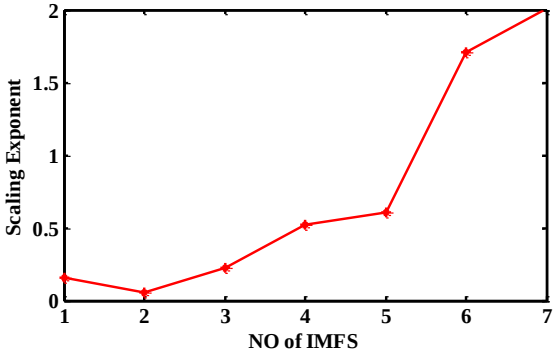

Figure 6. Scaling exponent (α) values for the 7 IMFs obtained after applying DFA technique to the 7 IMFs obtained by applying EMD method to the C/N$_0$ data received from the PRN 15 satellite on June 29, 2013.

Figure 7 shows the original GPS signal (blue in color) and reconstructed signal (green in color) after applying EMD-DFA technique. EMD-DFA algorithm was capable of mitigating 6.1dB of noise thereby decreasing errors. Around 18:00 Hrs (UT) C/N$_0$ ratio of original PRN15 satellite has fallen to 40.55dB-Hz due to ionospheric disturbances. Using EMD-DFA technique we are able to improve the C/N$_0$ ratio during 18:00 Hrs (UT).

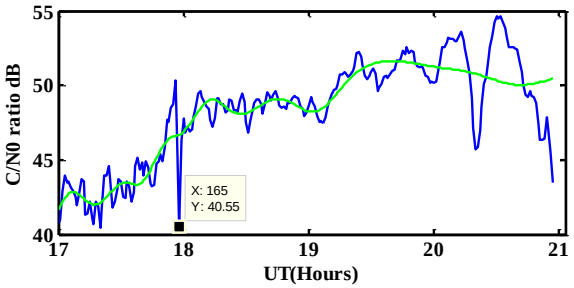

Figure 7. Raw GPS signal and the signal obtained by applying EMD-DFA technique for the data received from PRN 15 satellite on June 29, 2013.

VI. CONCLUSIONS

High-precision in carrier phase measurements is of great concern in order to obtain high accuracy in GPS positioning information but the carrier phase measurements mainly suffer from cycle slips problem. To detect the discontinuities in carrier phase measurements, a higher-order phase difference technique was used and for mitigation of scintillations and cycle slip effects on the received GPS signal EMD-DFA method was suggested. Cycle slips occurrence was observed at 18:00 Hrs (UT) on June 29, 2013 for PRN 15 satellite and a strong scintillation phenomenon of 0.8(S4) is observed at the same time indicating a correlation between cycle slip occurrence and ionospheric scintillations. On June 29, 2013, Dst index has fallen to -98 nT indicating the occurrence of geomagnetic storm. On this day, significant numbers of cycle slips are detected during the storm time. Geomagnetic activities result in ionosphere irregularities thereby degrading the quality of GPS signal and causing loss of lock. During the severe geomagnetic storms occurrence of cycle slips are enhanced in the solar maximum (2013) year. During equinox month, more cycle slips are detected when compared with other months. C/N$_0$ ratio of PRN15 satellite on June 29, 2013 has fallen to 40.55 dB at 18:00 Hrs (UT) due to ionospheric disturbances. EMD-DFA algorithm was capable of mitigating 6.1dB of noise. The outcome of this work would be useful for understanding the relation between cycle slips & scintillations to improve GNSS receiver design for accurate positioning using carrier phase measurements.

Acknowledgments and Data

This work was supported by the Department of Science and Technology, New Delhi, India, SR/FST/ESI-130/2013(C) FIST program and by the University Grants Commission (UGC), New Delhi, File No: F. 301/2013(SAII)/RA201416GEANP5585

REFERENCES

1. Hoffmann-Wellenhof, B., H. Lichtenegger, and J. Collins (1994), GPS theory and practice, Springer-Verlag, *New York*.
2. Leick, A., L. Rapoport, and D. Tatarnikov (2015), GPS satellite surveying, John Wiley & Sons.
3. Dai, Z. (2012), MATLAB software for GPS cycle-slip processing, GPS solutions, 16(2), 267-272.

Published By:
Blue Eyes Intelligence Engineering and Sciences Publication (BEIESP)

4. Skone, S., K. Knudsen, and M. De Jong (2001), Limitations in GPS receiver tracking performance under ionospheric scintillation conditions, Physics and Chemistry of the Earth, Part A: Solid Earth and Geodesy, 26 (6), 613-621.
5. Silva, P. (2013), Cycle Slip Detection and Correction for Precise Point Positioning, Proceedings of the Institute of Navigation ION GNSS, 22 (2015), 47.
6. Blewitt, G. (1990), Jet Propulsion Laboratory, California Institute of Technology, Pasadena, Geophysical Research Letters, 17(3), 199-202.
7. de Lacy, M. C., M. Reguzzoni, F. Sansò, and G. Venuti (2008), The Bayesian detection of discontinuities in a polynomial regression and its application to the cycle-slip problem, Journal of Geodesy, 82(9), 527-542.
8. Sunda, S., R. Sridharan, B. Vyas, P. Khekale, K. Parikh, A. Ganeshan, C. Sudhir, S. Satish, and M. S. Bagiya (2015), Satellite-based augmentation systems: A novel and cost-effective tool for ionospheric and space weather studies, Space Weather, 13 (1), 6-15.
9. Liu, Z. (2011), A new automated cycle slip detection and repair method for a single dual-frequency GPS receiver, Journal of Geodesy, 85(3), 171-183.
10. Dai, Z., S. Knedlik, and O. Loffeld (2009), Instantaneous triple-frequency GPS cycle-slip detection and repair, International Journal of Navigation and Observation.
11. Kim, D., and R. B. Langley, Instantaneous Real-Time Cycle-Slip Correction for Quality Control of GPS Carrier-Phase Measurements (2002), Navigation, vol. 49, pp. 205-222.
12. Banville, S., R. Langley, S. Saito, and T. Yoshihara (2010), Handling cycle slips in GPS data during ionospheric plasma bubble events, Radio Science, vol. 45.
13. Zhang, D., L. Cai, Y. Hao, Z. Xiao, L. Shi, G. Yang, and Y. Suo (2010), Solar cycle variation of the GPS cycle slip occurrence in China low-latitude region, Space Weather, 8(10).
14. Zhao, L., L. Li, Y. Liu, and N. Li (2014), Cycle slip detection and repair with triple frequency combination method, paper presented at 2014 IEEE/ION Position, Location and Navigation Symposium-PLANS 2014, IEEE.
15. Yue, X., W. S. Schreiner, N. M. Pedatella, and Y. H. Kuo (2016), Characterizing GPS radio occultation loss of lock due to ionospheric weather, Space Weather, 14 (4), 285-299.
16. Dejie Yu, Junsheng Cheng, Yu Yang (2003), Application of EMD method and Hilbert spectrum to the fault diagnosis of roller bearings, doi:10.1016/S0888-3270(03)00099-2.
17. Yih Jeng, Ming-Juin Lin, Chih-Sung Chen, and Yu-Huai Wang (2007), Noise reduction and data recovery for a VLF-EM survey using a nonlinear decomposition method, Geophysics,Vol. 72, No. 5, P. F223–F235.
18. Kantelhardt, J. W., S. A. Zschiegner, E. Koscielny-Bunde, S. Havlin, A. Bunde, and H. E. Stanley (2002), Multifractal detrended fluctuation analysis of nonstationary time series, Physica A: Statistical Mechanics and its Applications, 316(1), 87-114.
19. Saba, M. F., W. Gonzalez, and A. Clúa de Gonzalez (1997), Relationships between the AE, ap and Dst indices near solar minimum (1974) and at solar maximum (1979), Annales Geophysicae, pp. 1265-1270.
20. Afraimovich, E. L., V. V. Demyanov, T. N. Kondakova (2003), Degradation of GPS performance in geomagnetically disturbed conditions, GPS Solutions, No.7, 109–119.
21. Koster, J. R., Equatorial scintillation (1972), Planetary and Space Science, vol. 20, pp. 1999-2014.
22. Burke, W., L. Gentile, C. Huang, C. Valladares, and S. Su, Longitudinal variability of equatorial plasma bubbles observed by DMSP and ROCSAT-1 (2004), Journal of Geophysical Research: Space Physics, vol. 109.
23. Tanna, H., and K. Pathak, Multifractality due to long-range correlation in the L-band ionospheric scintillation S 4 index time series (2014), Astrophysics and Space Science, vol. 350, pp. 47-56.

Published By:
Blue Eyes Intelligence Engineering and Sciences Publication (BEIESP)